Self-organization of charged particles on a two-dimensional lattice subject to anisotropic Jahn-Teller-type interaction and three-dimensional Coulomb repulsion

T. Mertelj,[1,2] V. V. Kabanov,[1,3] J. Miranda Mena,[1] and D. Mihailovic[1,2]
[1]*Jozef Stefan Institute, Jamova 39, 1000 Ljubljana, Slovenia*
[2]*Faculty of Mathematics and Physics, University of Ljubljana, 1000 Ljubljana, Slovenia*
[3]*Department of Physics, Loughborough University, Loughborough LE11 3TU, United Kingdom*
(Received 23 March 2007; revised manuscript received 31 May 2007; published 30 August 2007)

Self-organization of charged particles on a two-dimensional lattice, subject to an anisotropic Jahn-Teller-type interaction and three-dimensional Coulomb repulsion, is investigated. In the mean-field approximation without Coulomb interaction, the system displays a phase transition of first order. In the presence of the Coulomb repulsion, the global phase separation becomes unfavorable and the system shows a mesoscopic phase separation, where the size of the charged regions is determined by the competition between the ordering energy and the Coulomb energy. The phase diagram of the system as a function of particle density and temperature is obtained by systematic Monte Carlo simulations. With decreasing temperature, a crossover from a disordered state to a state composed of mesoscopic charged clusters is observed. In the phase separated state, charged clusters with even number of particles are more stable than those with odd number of particles in a large range of particle densities. With increasing particle density at low temperatures, a series of crossovers between states with different cluster sizes is observed. Above half-filling, in addition to the low temperature clustering, another higher temperature scale, which corresponds to orbital ordering of particles, appears. We suggest that the diverse functional behavior observed in transition metal oxides can be thought to arise from the self-organization of this type.

DOI: 10.1103/PhysRevB.76.054523 PACS number(s): 74.20.−z, 74.25.−q, 74.72.−h, 05.10.Ln

I. INTRODUCTION

The presence of nanoscale inhomogeneities is ubiquitous in cuprate superconductors,[1–6] magnetoresistive manganites,[7–12] and other doped transition metal oxides.[13–15] Furthermore, there is an emerging consensus that doped charge carriers in oxides may phase segregate to form nanoscale textures. These are believed to be of importance for achieving their functional properties such as superconductivity in cuprates[5] and giant magnetoresistance in manganites.[16]

For cuprates, the idea of charge segregation appeared soon after the discovery of superconductivity.[17–19] In a doped semiconductor, the phase separation may have two different origins. The first is the chemical origin and is associated with the segregation of dopant atoms. This type of phase segregation is usually temperature independent and weakly dependent on external perturbation. Exceptions may appear due to the large mobility of dopant atoms at relatively high temperature.

If the mobility of impurity atoms is small, one might expect a pure electronic mechanism of phase separation. In this case, the electronic system is in thermodynamic equilibrium and competing phases are close in energy. This is typical for systems exhibiting a first order phase transition. Electronic phase separation is very often observed in magnetic semiconductors such as EuSe or EuTe.[20–22] Therefore, the idea of charge segregation in cuprate superconductors and in manganites is very often associated with magnetic degrees of freedom,[23–25] where the phase separation is discussed within the *t-J* model. In Refs. 26–29, phase separation was studied within the Hubbard model. The results are still controversial. In some cases, the *t-J* model displays clear static[23] or dynamic[24] phase separation. The situation is quite different for the Hubbard model. For example, the results of numerical simulations[29] suggest that the phase separation is absent at any set of parameters and for any size of the lattice. Nevertheless, all these models do not consider *long-range* Coulomb repulsion which has very strong effect on the phase separation.[19,30–35]

The long-range Coulomb repulsion, together with the surface energy, determines the topology of the two phase state. The charged carriers have the tendency toward spatial segregation, which is caused by the fact that the free energy density of the phase with finite density of carriers is lower than the free energy density of the undoped system. On the other hand, charge segregation leads to the charging effect because the dopant atoms are distributed uniformly in the system. Therefore, a strong electric field appears which has a tendency to mix the charged phases. In the low doping limit, there is a low concentration of charged droplets and they do not overlap. The system behaves as an insulator. When the concentration increases, the percolative transition to a new phase is expected.[16,36,37]

More recently, it was suggested that an interplay of a short-range lattice attraction and the long-range Coulomb repulsion could lead to the formation of short metallic or insulating strings of polarons.[38,39] This was mainly motivated by the observation of giant isotope effect in manganites and cuprates.[40,41] In Ref. 42, we suggested that an anisotropic mesoscopic Jahn-Teller interaction between electrons and $k \neq 0$ optical phonons might lead to the formation of carrier pairs and stripes. A slightly different approach, based on elasticity, was considered more recently for the case of manganites by Khomskii and Kugel[43] using the methods of Eremin *et al.*[44] and Lookman and co-workers.[45]

The fundamental question which we try and answer here is how charged particles order in the presence of anisotropic

Jahn-Teller-type interaction, particularly when their density becomes large. We consider charged particles on a two-dimensional (2D) square lattice subject to *only* the long-range Coulomb interaction and an anisotropic Jahn-Teller (JT) deformation. In the preliminary report, we have considered a narrow doping range but have found clear evidence of phase segregation and preferential formation of pairs.[32] Here, we extend this study over the full doping range.

In the mean-field (MF) approximation without Coulomb repulsion, the system displays a first order phase transition to an ordered state below some critical temperature. In the presence of Coulomb repulsion, global phase separation becomes unfavorable and the system shows a mesoscopic phase separation, where the size of charged regions is determined by the competition between the ordering energy and the Coulomb energy. Using Monte Carlo (MC) simulations, we show that the system can form many different mesoscopic textures, such as clusters and stripes, depending only on the magnitude of the Coulomb repulsion compared to the anisotropic lattice attraction and the density of charged particles. Surprisingly, in agreement with the previous report, a feature arising from the anisotropy introduced by the Jahn-Teller interaction is that in a wide part of the phase diagram, objects with even number of particles are found to be more stable than those with odd number of particles, which could be significant for superconductivity when tunneling is included.[36]

II. FORMULATION

The model proposed in Ref. 42 involves all interactions allowed by the symmetry. We consider a simplified version of the model, where only the interaction leading to the deformation of the B_{1g} symmetry is taken into account. The interaction with B_{2g} mode leads to similar effects and, therefore, for our purposes, we can restrict ourselves by considering B_{1g} mode only. As a result, the interacting part of the Hamiltonian has the form

$$H_{JT} = g\sum_{\mathbf{r},\mathbf{l}} \sigma_{3,\mathbf{l}}\{(r_x^2 - r_y^2)f_0(r)\}(b_{\mathbf{l}+\mathbf{r}}^{\dagger} + b_{\mathbf{l}+\mathbf{r}}). \tag{1}$$

Here, the Pauli matrix $\sigma_{3,\mathbf{l}}$ describes two components of the electronic doublet, and $f_0(r)$ is a symmetric function describing the range of the interaction. We omit the spin index in the sum, since we ignore spin structure at present. The resulting model could be easily reduced to a lattice gas model. This is performed using the Lang-Firsov transformation or, equivalently, the adiabatic approximation for the phonon field. Let us introduce the classical variable $\mathbf{\Phi_i} = (b_{\mathbf{i}}^{+} + b_{\mathbf{i}})/\sqrt{2}$ and minimize the energy as a function of $\mathbf{\Phi_i}$ in the presence of the harmonic term $\omega\Sigma_{\mathbf{i}}\mathbf{\Phi}_{\mathbf{i}}^2/2$. We obtain the deformation, which corresponds to the minimum energy,

$$\Phi_{\mathbf{i}}^{(0)} = -\sqrt{2}g/\omega\sum_{\mathbf{r}} \sigma_{3,\mathbf{i}+\mathbf{r}} f(\mathbf{r}), \tag{2}$$

where $f(\mathbf{r}) = (r_x^2 - r_y^2)f_0(r)$. Substituting $\mathbf{\Phi}_{\mathbf{i}}^{(0)}$ to the Hamiltonian in Eq. (1) and taking into account that the carriers are charged, we arrive to the lattice gas model. To formulate the model, we use a pseudospin operator S with $S=1$ to describe the occupancies of the two electronic levels n_1 and n_2. Here, $S^z=1$ corresponds to the state with $n_1=1$, $n_2=0$, $S_i^z=-1$ to $n_1=0$, $n_2=1$, and $S_i^z=0$ to $n_1=n_2=0$. Simultaneous occupancy of both levels is excluded due to the high on-site Coulomb repulsion (CR) energy. The Hamiltonian in terms of the pseudospin operator is given by

$$H_{JT-C}^{LG} = \sum_{\mathbf{i},\mathbf{j}} (V_l(\mathbf{i}-\mathbf{j})S_{\mathbf{i}}^z S_{\mathbf{j}}^z + V_c(\mathbf{i}-\mathbf{j})Q_{\mathbf{i}}Q_{\mathbf{j}}), \tag{3}$$

where $Q_{\mathbf{i}} = (S_{\mathbf{i}}^z)^2$. $V_c(\mathbf{m}) = e^2/\epsilon_0 am$ is the Coulomb potential, e is the charge of electron, ϵ_0 is the static dielectric constant, and a is the effective unit cell period. The anisotropic short-range attraction potential is given by

$$V_l(\mathbf{m}) = g^2/\omega\sum_{\mathbf{i}} f(\mathbf{i})f(\mathbf{m}+\mathbf{i}). \tag{4}$$

The attraction in this model is generated by the interaction of electrons with optical phonons. The radius of the attraction force is determined by the radius of the electron-phonon interaction and the dispersion of the optical phonons.[39]

A similar model can be formulated in the limit of the continuous media. In this case, the deformation is characterized by components of the strain tensor. For the two-dimensional case, we can define three components of the strain tensor: $e_1 = u_{xx} + u_{yy}$ transforming as the A_{1g} representation of the D_{4h} group, $\epsilon = u_{xx} - u_{yy}$ transforming as the B_{1g} representation, and $e_3 = u_{xy}$ transforming as the B_{2g} representation. These components of the tensor are coupled linearly with the twofold degenerate electronic state which transforms as the E_g or E_u representation of the point group. Similar to the case of interaction with optical phonons, we will keep the interaction with deformation of the B_{1g} symmetry, namely, ϵ only. The Hamiltonian without the Coulomb term has the form

$$H = \tilde{g}\sum_{\mathbf{i}} S_{\mathbf{i}}^z \epsilon_{\mathbf{i}} + \frac{1}{2}(A_1 e_{1,\mathbf{i}}^2 + A_2\epsilon_{\mathbf{i}}^2 + A_3 e_{3,\mathbf{i}}^2). \tag{5}$$

Here, A_j are the corresponding components of the elastic modulus tensor, and $\tilde{g}$ is the coupling constant of the charge carriers with the strain tensor. The components of the strain tensor are not independent[45] and obey the compatibility condition

$$\nabla^2 e_1(\mathbf{r}) - 4\partial^2 e_3(\mathbf{r})/\partial x\partial y = (\partial^2/\partial x^2 - \partial^2/\partial y^2)\epsilon(\mathbf{r}).$$

The compatibility condition leads to the long-range anisotropic interaction between polarons. To derive the Hamiltonian, we minimize Eq. (5) with respect to e_1 and e_3 taking into account the compatibility condition. The resulting Hamiltonian in the reciprocal space has the form

$$H = \tilde{g}\sum_{\mathbf{k}} S_{\mathbf{k}}^z \epsilon_{\mathbf{k}} + (A_2 + A_1 U(\mathbf{k}))\frac{\epsilon_{\mathbf{k}}^2}{2}. \tag{6}$$

The wave vector dependence of the potential is given by

$$U(\mathbf{k}) = \frac{(k_x^2 - k_y^2)^2}{k^4 + 8(A_1/A_3)k_x^2 k_y^2}. \quad (7)$$

By minimizing the energy with respect to ϵ_k and including the long-range CR, we again obtain Eq. (3). The anisotropic interaction potential $V_l(\mathbf{m}) = -\Sigma_{\mathbf{k}} \exp(i\mathbf{k}\cdot\mathbf{m}) \frac{\tilde{g}^2}{2(A_2 + A_1 U(\mathbf{k}))}$ is determined in this case by the interaction with the classical deformation and is long range as well. The potential $U(\mathbf{k})$ [Eq. (7)] depends on the direction of the wave vector $\hat{\mathbf{k}}$ only; therefore, $V_l(\mathbf{r})$ decays as $1/r^2$ at large distances.[46] Since attraction forces decay faster than the Coulomb repulsion at large distances, the attraction can overcome the Coulomb repulsion at short distances leading to the mesoscopic phase separation.

Irrespective of whether the resulting interaction between polarons is generated by acoustic or optical phonons, the main physical picture remains the same. In both cases, there is an anisotropic attraction between polarons over short distances. This interaction can be either ferromagnetic or antiferromagnetic in terms of the pseudospin operators depending on the spatial direction. Without losing generality, we assume that $V_l(\mathbf{m})$ is nonzero only for the nearest neighbors and can be either ferromagnetic or antiferromagnetic.

III. MEAN FIELD

Our main goal is to study this lattice gas model [Eq. (3)] at a constant average density,

$$n = \frac{1}{N} \sum_{\mathbf{i}} Q_{\mathbf{i}}, \quad (8)$$

where N is the total number of sites. However, to clarify the physical picture, we first perform calculations in the absence of long-range CR at a fixed chemical potential by adding the term $-\mu\Sigma_{\mathbf{i}} Q_{\mathbf{i}}$ to the Hamiltonian in Eq. (3).

Similar models were studied many years ago on the basis of the molecular-field approximation in the Bragg-Williams formalism.[47,48] The mean-field equations for the two variables n and $M = \frac{1}{N}\Sigma_{\mathbf{i}} S_{\mathbf{i}}^z$ have the forms[47]

$$M = \frac{2\sinh(2zV_l M/k_B T)}{\exp(-\mu/k_B T) + 2\cosh(2zV_l M/k_B T)}, \quad (9)$$

$$n = \frac{2\cosh(2zV_l M/k_B T)}{\exp(-\mu/k_B T) + 2\cosh(2zV_l M/k_B T)}. \quad (10)$$

Here, $z=4$ is the number of the nearest neighbors for the square lattice in two dimensions and k_B is the Boltzmann constant. For positive $\mu > 0$, Eq. (9) has two solutions below T_c. The solution with $M=0$ is unstable while the solution with a finite M corresponds to the global minimum with $n \to 1$ for $T \to 0$. When $-2zV_l < \mu < 0$, the equation has three solutions below $T_{c1} < T_c$. The free energy has two minima and one maximum. The phase transition at T_{c1} is of first order. The trivial solution $M=0$ corresponds to the case when $n \to 0$ as $T \to 0$. For $\mu < -2zV_l$, there is only the trivial solution of the equation $M=0$.

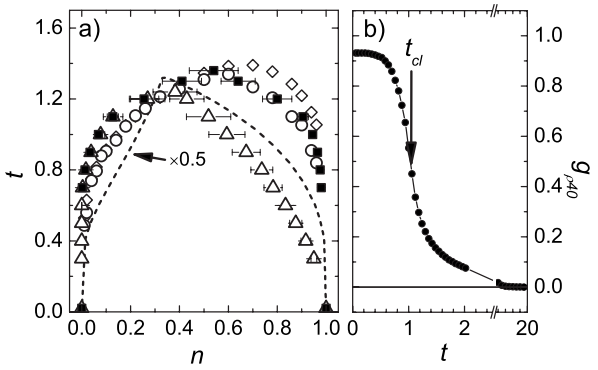

FIG. 1. (a) The phase diagram of the model in the absence of the Coulomb repulsion (Ref. 49). The dashed line represents the MF solution. The full squares (■) represent the $t_{crit}(n)$ line calculated for the periodic boundary conditions by means of the multicanonical MC algorithm with the system of size $L=40$. For comparison, the $t_{crit}(n)$ line is shown (△) for open boundary conditions. The $t_{cl}(n)$ lines for periodic (○) and open (◇) boundary conditions are also shown. (b) The dependence of the nearest neighbor density correlation function $g_{\rho L}$ on temperature in the absence of the Coulomb repulsion. The definition of $t_{cl}(n)$ is indicated by the arrow. The numerical error bars are of the order of the symbol sizes.

When the number of particles is fixed [Eq. (8)], the system is unstable with respect to global phase separation below $T_{crit}(n)$. The line of the phase transition is determined by the condition $F(M=0, \mu_{crit}(T), T) = F(M(T), \mu_{crit}(T), T)$, where F is the free energy, $\mu_{crit}(T)$ is the critical chemical potential, and M is the solution of Eq. (9). As a result, at a fixed average n, two phases with $n_0(T) = n(M=0, \mu_{crit}(T), T)$ and $n_M(T) = n(M(T), \mu_{crit}(T), T)$ coexist as determined by Eqs. (9) and (10). The region of phase coexistence is shown in Fig. 1.[49] For comparison with the MF solutions, we performed Monte Carlo simulations of the model [Eq. (3)] in the absence of the Coulomb forces. Due to strong fluctuations in two dimensions, the critical temperature determined from MC simulations is reduced by a factor of ~2 in comparison to the MF result.

IV. COULOMB FRUSTRATED FIRST ORDER PHASE TRANSITION

Let us now consider the role of the Coulomb repulsion. The area under the $T_{crit}(n)$ in Fig. 1 is the area of phase coexistence. If we fix the temperature, the two phases with the bulk concentrations n_0 and n_M will have volume fractions $1-x$ and x, respectively, where $x = (n-n_0)/(n_M - n_0)$. Since the system is globally electroneutral, the phases with n_0 and n_M are charged. However, a large increase of the Coulomb energy is required to break electroneutrality. As a consequence, growth of charged regions with two different charge densities is blocked by the Coulomb forces.

In the literature, there are a few examples of introduction of charging effects in the problem of phase separation.[32–35] There are several different possibilities to include long-range Coulomb forces in the model. Muratov[35] proposed that the

order parameter is a charged scalar and the charge density is proportional to the order parameter. This situation is similar to the problem of a charged Bose gas in magnetic field considered in Ref. 50. A similar situation is considered in Ref. 34, where the free energy has two distinct minima as a function of the density and gradient terms in the free energy are replaced by the surface tension. Jamei *et al.*[33] considered the case with a scalar order parameter where the charge density is coupled to the order parameter as an external field.

In our case, symmetry allows coupling of the charge density with the square of the order parameter only. Let us consider the classical free energy density corresponding to the first order phase transition:

$$F_1 = ((\tau - 1) + (\eta^2 - 1)^2)\eta^2. \tag{11}$$

Here, $\tau=(T-T_c)/(T_0-T_c)$ is the dimensionless temperature. At $\tau=4/3$ $(T=T_0+(T_0-T_c)/3)$, a nontrivial minimum in the free energy appears. At $\tau=1$ $(T=T_0)$, the first order phase transition occurs. Below $\tau=1$, the trivial solution $\eta=0$ corresponds to the metastable phase. At $\tau=0$ $(T=T_c)$, the trivial solution becomes unstable. In order to study the case of the Coulomb frustrated phase transition, we have to add coupling of the order parameter to the local charge density. In our case, the order parameter describes the sublattice orbital magnetization and, therefore, only the square of the order parameter can be coupled to the local 2D charge density ρ:

$$F_{coupl} = -\alpha\eta^2\rho. \tag{12}$$

The proposed free energy functional is similar to that proposed in Ref. 33. In our case, the charge plays the role of the local temperature, while in Ref. 33, there is a linear coupling of the charge to the order parameter and the charge density plays the role of the external field.

The total free energy density should also contain the gradient term and the electrostatic energy:

$$F_{grad} + F_{el} = C(\nabla\eta)^2 + \frac{1}{2}K[\rho(\mathbf{r}) - \bar{\rho}] \times \int d^2r'[\rho(\mathbf{r}') - \bar{\rho}]/|\mathbf{r} - \mathbf{r}'|. \tag{13}$$

Here, we write $\bar{\rho}$ explicitly to take into account global electroneutrality. The total free energy [Eqs. (11)–(13)] should be minimized at fixed τ and $\bar{\rho}$.

Next, we proceed to show that the Coulomb term leads to phase separation in two dimensions. Minimization of F with respect to the charge density $\rho(\mathbf{r})$ leads to the following equation:

$$-\alpha\nabla_{3D}^2\eta^2 = 4\pi K[\rho(\mathbf{r}) - \bar{\rho}]\delta(z). \tag{14}$$

Here, we write explicitly that the electrostatic field is three dimensional but the charge density $\rho(\mathbf{r})$ is confined in the 2D plane $(z=0)$. We believe that this condition is favorable for creating charge segregation because the electrostatic field is not screened in the third direction. Solving this equation by applying the Fourier transform and substituting the solution back into the free energy density, we obtain

$$F = F_1 - \alpha\eta^2\bar{\rho} + C(\nabla\eta)^2 - \frac{\alpha^2}{8\pi^2 K}\int d^2r' \frac{\nabla(\eta(\mathbf{r})^2)\,\nabla(\eta(\mathbf{r}')^2)}{|\mathbf{r} - \mathbf{r}'|}. \tag{15}$$

As a result, the free energy functional is similar to the case of first order phase transition with a shifted critical temperature due to the presence of the term $\alpha\eta^2\bar{\rho}$ and with an additional nonlocal gradient term.

To demonstrate that the uniform solution has a higher free energy than a nonhomogeneous solution, we make the Fourier transformation of the gradient term:

$$F_{grad} \propto Ck^2|\eta_{\mathbf{k}}|^2 - \frac{\alpha^2 k|(\eta^2)_{\mathbf{k}}|^2}{4\pi K}, \tag{16}$$

where $\eta_{\mathbf{k}}$ and $(\eta^2)_{\mathbf{k}}$ are Fourier components of the order parameter and square of the order parameter, respectively. If we assume that the solution is uniform, i.e., $\eta_0 \neq 0$ and $(\eta^2)_0 \neq 0$, small nonuniform corrections to the solution reduce the free energy at small $\mathbf{k}$, where the second term dominates.

In addition to the ordinary CR term, a charge compressibility term was introduced in Ref. 51. This term changes the relation between the order parameter and charge density [Eq. (14)] at large wave vectors (short distances) leading to the momentum independent relation $(\eta^2)_{\mathbf{k}} \propto \rho_{\mathbf{k}}$. On the other hand, it has a small effect on Eq. (14) in the long wavelength limit. Therefore, Eq. (16) remains unaffected by the charge compressibility in the long wavelength limit.

The situation is different in three dimensions. Direct solution of the equation for the charge density leads to the *local* gradient term of higher order, $-\frac{\alpha^2}{8\pi K}(\nabla\eta(\mathbf{r})^2)^2$. This term can also lead to instability, and higher order expansion in gradient terms becomes important.

V. MONTE CARLO SIMULATIONS

To substantiate the above arguments, we performed MC simulations of the system described by the Hamiltonian in Eq. (3) with and without the presence of the long-range CR. The simulations were performed on a square lattice with dimensions $L\times L$ sites with $10\leqslant L\leqslant 100$ at different dimensionless temperatures $t=k_BT\epsilon_0 a/e^2$. The short-range potential $v_l(\mathbf{i})=V_l(\mathbf{i})\epsilon_0 a/e^2$ was taken to be nonzero only for $|\mathbf{i}|=1$ and was therefore specified by a single parameter $v_l(1,0)$.

We first performed MC simulations of the model at a constant chemical potential in the absence of CR. Due to the presence of first order phase transition, the particle density probability distribution $P_{t,\mu}(n)$ has two peaks when the chemical potential is near the critical value $\mu_{crit}(t)$. At $\mu_{crit}(t)$, the two peaks have equal height corresponding to the densities of the two coexisting phases n_0 and n_M. A standard Metropolis algorithm,[52] in combination with simulated annealing[53] and histogram reweighting technique,[54] gave reliable results only at higher temperatures near maximum $t_{crit}(n)$. At lower temperatures the standard Metropolis simulation becomes strongly nonergodic. To improve ergodicity

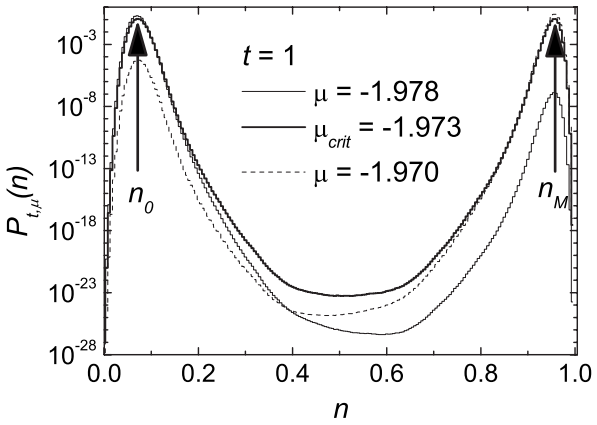

FIG. 2. Histograms of the density probability distribution $P_{t,\mu}(n)$ at the chemical potential near $\mu_{crit}(t)$ obtained by multicanonical MC simulation in the absence of Coulomb repulsion. The values of the coexisting densities n_0 and n_M at the given temperature are indicated by the arrows. Note the logarithmic scale.

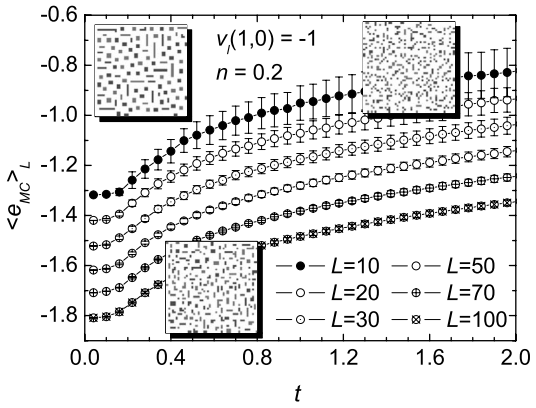

FIG. 3. A typical temperature dependence of the average energy per particle estimator $\langle e_{MC}\rangle_L$ for different system sizes L. The insets show snapshots of particle distribution at different temperatures, where the darker and brighter shades of gray represent $S_i^z=1$ and -1, respectively. The curves are vertically shifted for 0.1; the error bars represent $\sigma_{e_{MC}}$.

we used a variant of multicanonical approach[55] adapted to uniformly sample states over the full range of densities[56] n at a constant dimensionless temperature t_{sim} and chemical potential μ_{sim}. At each temperature, the final histogram acquisition run involved at least 10^6 MC pseudospin flips per site. The density probability histograms $P_{t_{sim},\mu}(n)$ for several values of the chemical potential μ close to the simulation chemical potential μ_{sim} were then calculated at each t_{sim} by reweighting[54] (see Fig. 2). From the histogram with equal peak heights, the densities of the two coexisting phases n_0 and n_M were then determined at a given t_{sim}.

In simulations at constant n, one MC step consisted of a single update per particle, where the trial move consisted of setting $S_z=0$ at the site with nonzero $Q_\mathbf{i}$ and $S_z=\pm 1$ at a randomly selected site with zero $Q_\mathbf{i}$. A standard Metropolis algorithm,[52] in combination with simulated annealing,[53] was used in this case. A typical simulated annealing run consisted of a sequence of MC simulations at different temperatures. At each temperature, equilibration phase consisting of 10^3-10^6 MC steps was first executed followed by the averaging phase consisting of the same or greater number of MC steps. Observables were measured after each MC step during the averaging phase only.

At constant n in the absence of the CR, global phase separation below $t_{crit}(n)$ occurs in the form of a large cluster with $M\neq 0$. To detect onset of clustering, we measure the nearest neighbor density correlation function (CF) $g_{\rho L}=\frac{1}{4n(1-n)L^2}\Sigma_{|\mathbf{m}|=1}\langle\Sigma_\mathbf{i}(Q_{\mathbf{i}+\mathbf{m}}-n)(Q_\mathbf{i}-n)\rangle_L$, where $\langle\ \rangle_L$ represents the MC average. We define the temperature $t_{cl}(n)$ at which $g_{\rho L}$ rises to 50% of its low temperature value [see Fig. 1(b)] as the characteristic crossover temperature related to the formation of clusters.

In Fig. 1(a), we show the results of MC simulations in the absence of the Coulomb repulsion. We find that for $n\gtrsim 0.4$, the boundary conditions strongly affect the $t_{crit}(n)$ line calculated at the constant chemical potential. When we use open boundary conditions (OBC), $t_{crit}(n)$ is strongly suppressed above $n\approx 0.4$ in comparison to the result obtained with the periodic boundary conditions (PBC). At constant n, on the other hand, the influence of the boundary conditions on $t_{cl}(n)$ is less pronounced. The $t_{cl}(n)$ calculated with both types of boundary conditions closely follow the $t_{crit}(n)$ line calculated with PBC. Above $n\approx 0.6$, $t_{cl}(n)$ for OBC is only slightly higher than that for PBC. We attribute the insensitivity of $t_{cl}(n)$ to boundary conditions at fixed n to sensitivity of the correlation function to the short-range correlations which are less sensitive to boundary conditions.

Next, we analyze the model in the presence of the long-range CR at constant n. In Fig. 3, we show a typical temperature dependence of the average energy per particle estimator $\langle e_{MC}\rangle_L$ for different system sizes L in the presence of the long-range CR using OBC. Error bars represent the standard deviation $\sigma_{e_{MC}}=\sqrt{\langle e_{MC}^2\rangle_L-\langle e_{MC}\rangle_L^2}$. The average energy monotonously drops with decreasing temperature. The drop is more pronounced in the temperature interval $\sim 0.5>t>\sim 0.1$ in which clusters start to form. Below $t\sim 0.1$, the clusters are partially ordered. The temperature dependence of $\langle e_{MC}\rangle_L$ is virtually identical for all L (we should note that the curves are vertically shifted by 0.1 for clarity) indicating that the boundary effects on $\langle e_{MC}\rangle_L$ are negligible even for the smallest system sizes.

In the temperature region where clusters partially order, the heat capacity $c_L=\partial\langle e_{MC}\rangle_L/\partial t$ displays the peak at $t_{co}(n)$ [see Fig. 5(b)]. The peak displays no scaling with L indicating that no long-range ordering of clusters appears. Inspection of the particle distribution snapshots at low temperatures[32] reveals that finite size domains form (see Fig. 6). Within the domains, the clusters are ordered. The domain wall dynamics seems to be much slower than our MC simulation time scale, preventing domains from growing. The effective L is therefore limited by the domain size. This explains the absence of the scaling and clear evidence for a phase transition near $t_{co}(n)$. From the simulations, it is therefore not clear whether the absence of complete cluster ordering is due to the finiteness of the MC simulation or also due

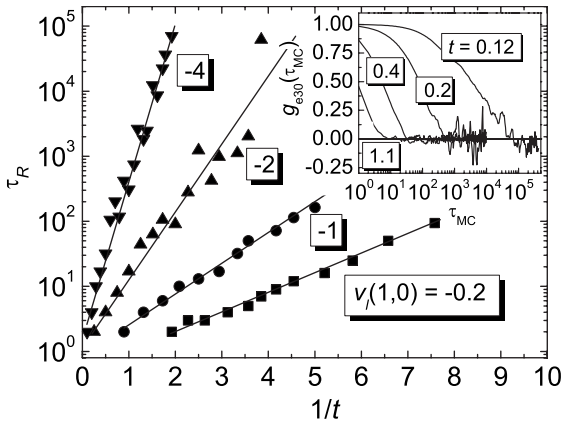

FIG. 4. The characteristic MC relaxation time τ_R as a function of temperature for different values of $v_l(1,0)$. The thin lines represent the Arrhenius fits. The inset shows the autocorrelation function $g_{e30}(\tau_{MC})$ at a few temperatures for $v_l(1,0)=-1$. For convenience, τ_R is defined as a value of τ_{MC} where $g_{eL}(\tau_{MC})=0.25$.

to the glassy form of the free energy landscape. The square shape of the sample may frustrate the cluster orders with nontetragonal symmetries, while a practically achievable number of MC steps per temperature step warrants reliable MC averages only above the temperature which is of the same order as $t_{co}(n)$. The cluster ordering temperature $t_{co}(n)$, which is the lowest energy scale at all densities, is only weakly n dependent in the range $0.1 \lesssim n \lesssim 0.9$.

To check the convergence of our simulations, we analyzed the MC update dynamics by calculating the autocorrelation function of energy fluctuations,

$$g_{eL}(\tau_{MC}) = \frac{1}{K\sigma^2_{e_{MC}}} \sum_{i=1}^{K} (e_{MC}(i+\tau_{MC}) - \langle e_{MC}\rangle_L)(e_{MC}(i) - \langle e_{MC}\rangle_L), \quad (17)$$

where $e_{MC}(i)$ represents the energy per site at the ith MC step and τ_{MC} represents the MC time. A typical time dependence of $g_{eL}(\tau_{MC})$ is shown in the inset in Fig. 4. The autocorrelation function drops with the characteristic MC relaxation time τ_R. $1/\tau_R$ displays Arrhenius temperature dependence (see Fig. 4) down to the temperature where clusters start to order. Below this temperature, τ_R behaves more erratically. The activation energy strongly depends on the magnitude of the short-range potential $v_l(1,0)$. The lowest temperature for which our simulation gives reliable results therefore strongly depends on the magnitude of the short-range potential due to the limited number of steps in the MC production runs. For our choice of the short-range potential strength, the achievable number of steps was large enough to ensure convergence for all temperatures down to $t_{co}(n)$.

We now set $v_l(1,0)=-1$ and study the dependence of clustering on particle density. To detect clustering, we again use the nearest neighbor CF. In Fig. 5(c), we plot a typical nearest neighbor CF, $g_{\rho 40}(1,0)$, as a function of temperature. At high temperatures $t \gg |v_l(1,0)|$, CF is slightly negative due to the long-range CR. When the temperature decreases,

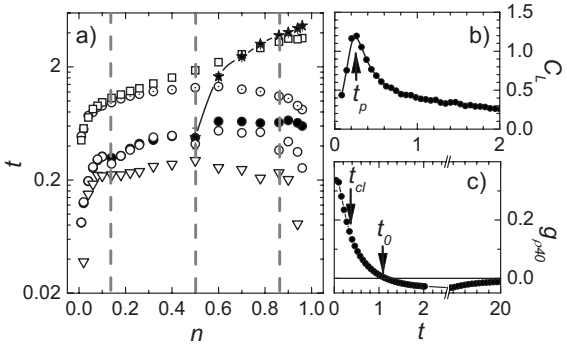

FIG. 5. (a) The phase diagram of the model in the presence of the long-range Coulomb repulsion. The open circles (○) and full circles (●) represent the $t_{cl}(n)$ line for periodic and open boundary conditions, respectively, while the dotted circles (⊙) represent the $t_{cl}(n)$ line for periodic boundary conditions in the absence of the long-range CR. The onset of clustering, $t_0(n)$, is shown by the open squares (□) and the cluster ordering temperature $t_{co}(n)$ by the open triangles (Δ). The pseudospin (orbital) ordering temperature is shown by the full stars (⋆). Note the logarithmic scale. The error bars are of the order of the symbol sizes or smaller. (b) The definition of t_p from the peak in the temperature dependence of the heat capacity. (c) The definitions of t_0 and t_{cl} from the temperature dependence of the nearest neighbor density correlation function.

CF becomes positive and further rises with the decreasing temperature. No saturation of CF as in the case of the absence of the CR forces is observed with the decreasing temperature [see Fig. 1(b)]. Again, we define the temperature at which CF rises to 50% of its low temperature value as the characteristic crossover temperature $t_{cl}(n)$ related to the formation of clusters. The dependence of $t_{cl}(n)$ on the particle density is shown in Fig. 5(a) for different boundary conditions. While in the absence of the long-range CR $t_{cl}(n)$ closely follows the $t_{crit}(n)$ line [Fig 1(a)], suppression of clustering by the CR forces results in a significant decrease of $t_{cl}(n)$.

Different boundary conditions influence $t_{cl}(n)$ only for densities above $n \gtrsim 0.5$. In this region, the particles that form clusters are holes ($Q_{\mathbf{i}}=0$) in the background of pseudospins ($Q_{\mathbf{i}}=1$). The open boundary conditions are effectively a perimeter formed from holes which attracts holes and, by pinning, enhances hole clustering, resulting in an increase of $t_{cl}(n)$ for OBC.

In addition, for $n \geqslant 0.5$ and our choice of $v_l(\mathbf{i})$, the pseudospin background ferromagnetically orders at $t_S(n)$, which increases with increasing density, as shown in Fig. 5(a). The pseudospin ordering temperature is significantly higher than $t_{cl}(n)$. Despite this, the particle-hole symmetry of the $t_{cl}(n)$ line is absent. The absence of the particle-hole symmetry is a consequence of different entropy contributions of doubly degenerate particle level ($S_{\mathbf{i}z}=\pm 1$ for $Q_{\mathbf{i}}=1$) and singly degenerate hole level ($S_{\mathbf{i}z}=0$ for $Q_{\mathbf{i}}=0$).

The $t_{cl}(n)$ line does not appear smooth. There are clear dips at $n \approx 0.14$, $n=0.5$, and $n \approx 0.86$. With increasing density, the ground state of the system apparently goes through a series of crossovers related to the most probable cluster sizes, as shown in Fig. 6. While the dip at half-filling clearly cor-

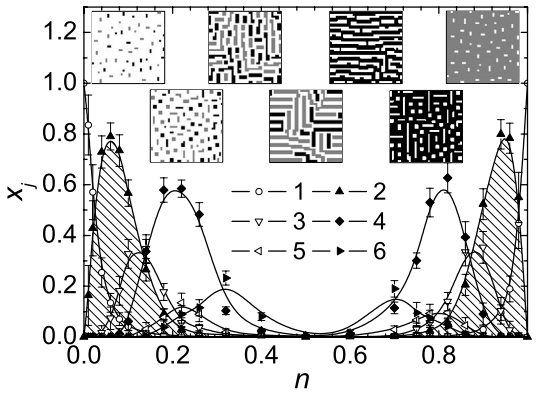

FIG. 6. The density dependence of the cluster-size distribution function x_j for a few of the smallest cluster sizes as a function of the average density at the temperature $t=0.14$. The regions of densities where pairs prevail are shadowed.

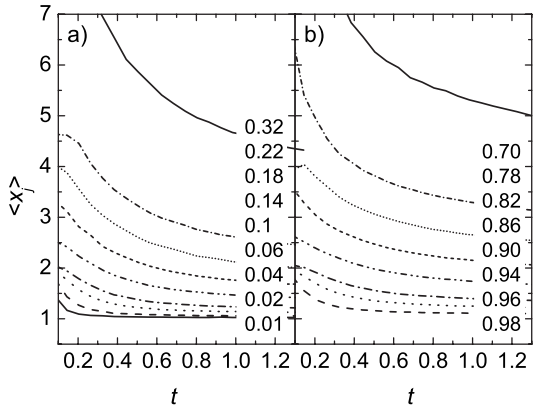

FIG. 7. The temperature dependence of the average cluster size for different particle densities n (a) below half-filling (particle clusters) and (b) above half-filling (hole clusters).

responds to commensurate ordering of stripes, the other two dips approximately correspond to the densities at which clusters of size 4 start to replace pairs (see Fig. 6). There is no obvious commensuration to the underlying lattice at these densities. At densities at which larger clusters start to replace quartets, no comparable anomaly is observed in the $t_{cl}(n)$ line.

Despite the presence of the CR forces, some clusters already start to form at temperatures higher than $t_{cl}(n)$. We can estimate the upper limit for the onset of cluster formation by the temperature $t_0(n)$ at which $g_{\rho L}(1,0)$ crosses 0. It is interesting that $t_0(n)$ almost coincides with the $t_{crit}(n)$ line [see Fig. 5(a)] below $n \lesssim 0.4$, while at higher densities, the onset of clustering appears at much higher temperatures. In the region $0.5 < n \lesssim 0.75$, the temperature at which the onset of clustering occurs is higher than the pseudospin ordering temperature $t_S(n)$, while above $n \approx 0.75$, the pseudospin ordering represents the highest energy scale.

To get further insight into the cluster formation, we measured the cluster-size distribution function. In Fig. 6, we show the low temperature density dependence of the cluster-size distribution function, $x_j = N_p(j)/(nL^2)$, where $N_p(j)$ is the number of particles for $n \leqslant 0.5$ or holes for $n > 0.5$ in clusters of size j. At the highest temperature, x_j is close to the distribution expected for the random ordering. When the temperature decreases, the number of larger clusters starts to increase at the expense of the single particle number.[32] Further down in temperature, depending on the average density n, clusters of a certain size start to prevail at the expense of all other sizes. Depending on the particle density, prevailing clusters can be pairs up to $n \approx 0.14$, quartets up to $n \approx 0.3$, etc. The situation is qualitatively symmetrical for the clusters formed by holes at $n > 0.5$. The preference for clusters with an even number of particles is not very sensitive to the shape of the anisotropic attractive potential. However, some nearly isotropic choices of $v_l(i,j)$ do not show the preference for an even number of particles in a cluster.

Analysis of binding energies of isolated clusters with various numbers of particles did not reveal any systematics that would lead to a simple explanation of the even-number preference. The observed behavior is therefore not just a consequence of anisotropy of $v_l(i,j)$ but also of a subtle interplay between the lattice topology and correlations due to the long-range Coulomb repulsion.

It should also be emphasized that the preference to certain cluster sizes becomes clearly apparent only at temperatures lower than $t_{cl}(n)$; however, the transition is not abrupt but gradual with decreasing temperature. This is also seen from the gradual increase of the average cluster size with decreasing temperature shown in Fig. 7. Around half-filling, the average cluster size starts to diverge at low temperatures, indicating formation of long stripelike objects (see insets in Fig. 6) and proximity of the percolation.

VI. CONCLUSIONS

We presented the results of extensive investigation of the ordering of charged Jahn-Teller polarons as a function of doping and temperature. We consider charged particles on a 2D square lattice subject to only the long-range Coulomb interaction and an anisotropic JT deformation.

We prove that without the long-range Coulomb repulsion, the system is unstable with respect to the first order phase transition below the density dependent critical temperature. This was demonstrated by the solution of the mean-field equation, as well as by direct Monte Carlo simulations. It was shown that this result does not depend on the type of boundary conditions and the error due to finite size effect is estimated.

In the presence of the Coulomb repulsion, the global phase separation becomes unfavorable and the system shows a mesoscopic phase separation, where the size of the charged regions is determined by the competition between the ordering energy and the Coulomb energy. The phenomenological theory of this effect was formulated where the square of the order parameter is coupled with the charge density. The charge density plays the role of the local temperature. This type of coupling is more general in comparison with the models where the charge plays the role of an external field.

Using MC simulations, we showed that below a characteristic clustering temperature, the system forms many differ-

ent mesoscopic textures, such as clusters and stripes, depending only on the magnitude of the Coulomb repulsion compared to the anisotropic lattice attraction and the density of charged particles. Below the clustering temperature, the system goes through a series of crossovers between phases with different mesoscopic textures when the particle density is increased. The low temperature part of the phase diagram is rather symmetric with respect to half-filling. However, above half-doping, another high temperature scale appears corresponding to orbital ordering of the particles. Surprisingly, a feature arising from the anisotropy introduced by the Jahn-Teller interaction is that objects with an even number of particles are more stable than those with an odd number of particles. Such a behavior could have significant implications for superconductivity when tunneling is included.[36]

ACKNOWLEDGMENTS

Enlightening discussions with A. S. Alexandrov, A. R. Bishop, C. DiCastro, L. P. Gorkov, F. Kusmartsev, and R. F. Mamin are highly appreciated. This work was supported within the FP6, Project No. NMP4-CT-2005-517039 (CoMePhS).

[1] R. J. McQueeney, Y. Petrov, T. Egami, M. Yethiraj, G. Shirane, and Y. Endoh, Phys. Rev. Lett. **82**, 628 (1999).
[2] A. Bianconi, N. L. Saini, A. Lanzara, M. Missori, T. Rossetti, H. Oyanagi, H. Yamaguchi, K. Oka, and T. Ito, Phys. Rev. Lett. **76**, 3412 (1996); E. S. Bozin, G. H. Kwei, H. Takagi, and S. J. L. Billinge, *ibid.* **84**, 5856 (2000).
[3] S. H. Pan *et al.*, Nature (London) **413**, 282 (2001); McElroy, R. W. Simmonds, J. E. Hoffman, D. H. Lee, J. Orenstein, H. Eisaki, S. Uchida, and J. C. Davis, *ibid.* **422**, 592 (2003).
[4] J. Demsar, B. Podobnik, V. V. Kabanov, T. Wolf, and D. Mihailovic, Phys. Rev. Lett. **82**, 4918 (1999); see also review by D. Mihailovic and V. V. Kabanov, in *Superconductivity*, ACS Series on Structure and Bonding, edited by A. Bussmann-Holder and K. A. Müller (Springer-Verlag, Berlin, 2004).
[5] See also D. Mihailovic and K. A. Müller, in *High T_c Superconductivity 1996: Ten Years After the Discovery*, edited by E. Kaldis, E. Liarokapis, and K. A. Müller, NATO Advanced Studies Institute, Series E: Applied Science (Kluwer, 1997), Vol. 343, p. 243.
[6] E. Dagotto, Rev. Mod. Phys. **66**, 763 (1994).
[7] J. M. De Teresa, M. R. Ibarra, P. A. Algarabel, C. Ritter, C. Marquina, J. Blasco, J. García, A. del Moral, and Z. Arnold, Nature (London) **386**, 256 (1997).
[8] G. Allodi, R. De Renzi, G. Guidi, F. Licci, and M. W. Pieper, Phys. Rev. B **56**, 6036 (1997).
[9] M. Uehara, S. Mori, C. H. Chen, and S.-W. Cheong, Nature (London) **399**, 560 (1999).
[10] M. Fath, S. Freisem, A. A. Menovsky, Y. Tomioka, J. Aarts, and J. A. Mydosh, Science **285**, 1540 (1999).
[11] G. Papavassiliou, M. Fardis, M. Belesi, T. G. Maris, G. Kallias, M. Pissas, D. Niarchos, C. Dimitropoulos, and J. Dolinsek, Phys. Rev. Lett. **84**, 761 (2000).
[12] Y. Kawasaki, T. Minami, Y. Kishimoto, T. Ohno, K. Zenmyo, H. Kubo, T. Nakajima, and Y. Ueda, Phys. Rev. Lett. **96**, 037202 (2006).
[13] P. L. Kuhns, M. J. R. Hoch, W. G. Moulton, A. P. Reyes, J. Wu, and C. Leighton, Phys. Rev. Lett. **91**, 127202 (2003).
[14] M. H. Sage, G. R. Blake, G. J. Nieuwenhuys, and T. T. M. Palstra, Phys. Rev. Lett. **96**, 036401 (2006).
[15] S.-W. Cheong, H. Y. Hwang, C. H. Chen, B. Batlogg, L. W. Rupp, Jr., and S. A. Carter, Phys. Rev. B **49**, 7088 (1994).
[16] E. Dagotto, T. Hotta, and A. Moreo, Phys. Rep. **344**, 1 (2001).
[17] J. Zaanen and O. Gunnarsson, Phys. Rev. B **40**, 7391 (1989).
[18] V. J. Emery, S. A. Kivelson, and O. Zachar, Phys. Rev. B **56**, 6120 (1997).
[19] L. P. Gorkov and A. V. Sokol, Pis'ma Zh. Eksp. Teor. Fiz. **46**, 333 (1987); L. P. Gorkov, J. Supercond. **14**, 365 (2001).
[20] J. Vitins and P. Wachter, Phys. Rev. B **12**, 3829 (1975).
[21] Y. Shapira, S. Foner, N. F. Oliveira, Jr., and T. Reed, Phys. Rev. B **5**, 2647 (1972).
[22] Y. Shapira, S. Foner, N. F. Oliveira, Jr., and T. Reed, Phys. Rev. B **10**, 4765 (1974).
[23] V. J. Emery, S. A. Kivelson, and H. Q. Lin, Phys. Rev. Lett. **64**, 475 (1990).
[24] V. J. Emery and S. A. Kivelson, Physica C **209**, 597 (1993).
[25] G. S. Uhrig and R. Vlaming, Phys. Rev. Lett. **71**, 271 (1993).
[26] A. Angelucci and S. Sorella, Phys. Rev. B **47**, 8858 (1993).
[27] A. Singh, Z. Tesanovic, and J. H. Kim, Phys. Rev. B **44**, 7757 (1991).
[28] Y. Bang, G. Kotliar, C. Castellani, M. Grilli, and R. Raimondi, Phys. Rev. B **43**, 13724 (1991).
[29] A. Moreo, D. Scalapino, and E. Dagotto, Phys. Rev. B, **43**, 11442 (1991).
[30] U. Löw, V. J. Emery, K. Fabricius, and S. A. Kivelson, Phys. Rev. Lett. **72**, 1918 (1994).
[31] J. Lorenzana, C. Castellani, and C. Di Castro, Phys. Rev. B **64**, 235127 (2001); Europhys. Lett. **57**, 704 (2002).
[32] T. Mertelj, V. V. Kabanov, and D. Mihailovic, Phys. Rev. Lett. **94**, 147003 (2005).
[33] R. Jamei, S. Kivelson, and B. Spivak, Phys. Rev. Lett. **94**, 056805 (2005).
[34] C. Ortix, J. Lorenzana, and C. Di Castro, Phys. Rev. B **73**, 245117 (2006).
[35] C. B. Muratov, Phys. Rev. E **66**, 066108 (2002).
[36] D. Mihailovic, V. V. Kabanov, and K. A. Muller, Europhys. Lett. **57**, 254 (2002).
[37] A. S. Alexandrov, A. M. Bratkovsky, and V. V. Kabanov, Phys. Rev. Lett. **96**, 117003 (2006).
[38] F. V. Kusmartsev, Phys. Rev. Lett. **84**, 530 (2000); **84**, 5026 (2000).
[39] A. S. Alexandrov and V. V. Kabanov, Pis'ma Zh. Eksp. Teor. Fiz. **72**, 825 (2000) [JETP Lett. **72**, 569 (2000)].
[40] G. M. Zhao, K. Conder, H. Keller, and K. A. Muller, Nature (London) **381**, 676 (1996).
[41] G. M. Zhao, M. B. Hunt, H. Keller, and K. A. Muller, Nature (London) **385**, 236 (1997).

[42] D. Mihailovic and V. V. Kabanov, Phys. Rev. B **63**, 054505 (2001); V. V. Kabanov and D. Mihailovic, *ibid.* **65**, 212508 (2002); V. V. Kabanov and D. Mihailovic, J. Supercond. **13**, 959 (2000).

[43] D. I. Khomskii and K. I. Kugel, Europhys. Lett. **55**, 208 (2001); Phys. Rev. B **67**, 134401 (2003).

[44] M. B. Eremin, A. Yu. Zavidonov, and B. I. Kochelaev, Zh. Eksp. Teor. Fiz. **90**, 537 (1986).

[45] S. R. Shenoy, T. Lookman, A. Saxena, and A. R. Bishop, Phys. Rev. B **60**, R12537 (1999); T. Lookman, S. R. Shenoy, K. O. Rasmussen, A. Saxena, and A. R. Bishop, *ibid.* **67**, 024114 (2003); K. H. Ahn, T. Lookman, and A. R. Bishop, Nature (London) **428**, 401 (2004).

[46] After the substitution $kr=u$, the potential is written as $1/r^2 \int \exp(iu\cos(\varphi))f(\varphi)ududu\varphi$.

[47] J. Lajzerovicz and J. Sivardiere, Phys. Rev. A **11**, 2079 (1975).

[48] J. Sivardiere and J. Lajzerovicz, Phys. Rev. A **11**, 2090 (1975).

[49] Even in the absence of Coulomb repulsion, we define dimensionless temperature in units of Coulomb energy $t=k_BT\epsilon_0 a/e^2$ and set the nearest neighbor short-range potential to $v_l(1,0)=V_l(1,0)\epsilon_0 a/e^2=-1$.

[50] V. V. Kabanov and A. S. Alexandrov, Phys. Rev. B **71**, 132511 (2005).

[51] C. Ortix, J. Lorenzana, M. Beccaria, and C. Di Castro, Phys. Rev. B **75**, 195107 (2007).

[52] N. Metropolis, A. W. Rosenbluth, M. N. Rosenbluth, A. H. Teller, and E. Teller, J. Chem. Phys. **21**, 1087 (1953).

[53] S. Kirkpatrick, C. D. Gelatt, and M. P. Vecchi, Science **220**, 671 (1983).

[54] A. M. Ferrenberg and R. H. Swendsen, Phys. Rev. Lett. **61**, 2635 (1988).

[55] B. A. Berg and T. Neuhaus, Phys. Lett. B **267**, 249 (1991).

[56] G. Orkoulas and A. Z. Panagiotopoulos, J. Chem. Phys. **110**, 1581 (1999).